Spatial Scale-dependent Effects of Tropical Cyclone Damage Functions over China

Rumei Tang[1], Jidong Wu[1, 2, *] and Juan Nie[3]

[1] State Key Laboratory of Earth Surface Processes and Resource Ecology, Beijing Normal University, Beijing 100875, China.

[2] School of National Safety and Emergency Management, Beijing Normal University, Beijing 100875, China.

[3] National Disaster Reduction Center of China, Ministry of Emergency Management, Beijing 100124, China

[*]Corresponding author: Jidong Wu (wujidong@bnu.edu.cn)

Key Points:

- The structure, parameters, and performance of the Tropical cyclone (TC) damage functions vary with spatial scale.
- Wind-calibrated sigmoidal damage function may lead to significant bias due to the neglect of TC-induced precipitation contributions.
- Integrated power-law model complements sigmoidal damage function giving better considering hazard, exposure, and vulnerability.

Abstract

Tropical cyclones (TCs) and their economic cost risk under climate change are significant concerns globally. Previous studies on TC damage functions and risk assessment are mostly performed based on modeling TC-level damage and thus obtaining the annual average loss for a country or region. The scalability of these damage functions at finer scales has been less systematically explored. In this study, we examine how the model structure, estimated parameters, and model performance of TC damage functions vary with spatial scale. The comparisons are illustrated by fitting two types of damage functions based on reported damage data at the county, province, and TC scales. We find that the newly proposed precipitation-calibrated sigmoidal damage function significantly outperforms the wind-calibrated sigmoidal damage function at three scales of county, province and TC event. Another type of power-law damage function that integrates hazard, exposure, and vulnerability complements the typical sigmoidal damage function because it yields a better fit when estimating direct economic loss above the province scale. Our work provides an empirical assessment of the role of spatial scale and damage function in TC economic impact evaluation and demonstrates the importance of spatially scale-specific policy-making in TC risk management and climate adaptation strategies.

Plain Language Summary

Tropical cyclones (TCs), as typical extreme events in the warming climate, cause damage to buildings and infrastructures, and therefore significant economic loss. The function that relates the TC intensity to the economic loss is called TC damage function (DF). TC damage function can be categorized into two types: the sigmoidal function accounts for wind-speed distribution, and the power-law function relates losses to maximum wind speed. Both types are usually used to model the loss in all TC-affected areas of a country. However, it is questionable whether these DFs are applicable to finer scales. We wonder how spatial scale affect the structure, parameters, and performance of TC damage function. We used reported damage data

at the county-, province-, and TC-scale in China to explore it. Results first showed that the difference brought by type of DF is greater than that due to the spatial scale. The typical sigmoidal DF using wind intensity may lead to bias due to the neglect of TC-induced precipitation. Different types of DF are suitable for different scales. And different driving forces of damage are reflected at different scales. Such spatial scale dependence of TC damage function could be instructive in multi-scale TC risk analysis and management.

1 Introduction

Tropical cyclones (TCs) pose a major threat to both coastal and inland areas at a global scale, affecting 22 million people and causing annual average direct economic losses ranging from USD 29 to 89 billion (Eberenz et al., 2021; Geiger et al., 2018). A few studies agree that TCs may become stronger while debating whether and how TC frequency will change under a warming climate (Bhatia et al., 2018; Emanuel, 2013; Knutson et al., 2010; Walsh et al., 2016). In addition to the uncertainty of TC characteristics, due to the increasing exposed population and assets and changing vulnerability, there is a need to determine the potential risk from TCs for decision-makers at different levels, especially when TC risk is expressed by direct economic loss (DEL). Additionally, it is a fact that TC impacts for an individual event are felt over smaller areas, which can be corroborated by the tendency of a higher resolution of the hazard and exposure datasets used in risk analysis (Ward et al., 2020). Thus, there is still a large gap in understanding the economic impact of TCs at different spatial scales.

Previous studies on modeling or predicting the economic impact of TCs can be classified into two groups according to the type of damage function used. The first type of damage function is sigmoidal curve-based, and the sigmoidal damage function proposed by Emanuel (2011) is a typical one. The TC damage function for the

77 spatially explicit modeling of the fraction of the property value damaged is
78 constrained by a specified minimum threshold and an upper bound of 100% damage
79 (Eberenz et al., 2021). The second type of damage function is power-law based.
80 Pielke (2007) suggested a high power-law dependence of damage based on wind
81 speed and first estimated future economic damage from TCs assuming damage as
82 being proportional to the third, sixth, and ninth powers of wind speed. The empirical
83 results presented by Nordhaus (2010) show that damage rises with the ninth power of
84 maximum wind speed. The fundamental difference between these two types of
85 damage functions is that the sigmoidal function accounts for local characteristics of
86 the full wind-speed distribution, while the power-law function attributes losses solely
87 to maximum wind speed at landfall in most cases. Geiger et al. (2016) referred to
88 these two forms of damage function as *local* and *global*, respectively.
89
90 Due to the limitations in the resolution of damage data reported for historical TC
91 events, most studies have carried estimations at TC event scales, and therefore, most
92 damage functions are also based on the TC scale. However, with the rapid
93 socioeconomic development of coastal areas and the growing availability of detailed
94 damage data, the need to understand physical risks from TCs at the province or county
95 scale is increasingly expressed by coastal governments, investors, and companies. In
96 addition to the need for practical disaster management, on the one hand, it is
97 questionable using only landfall or maximum wind speed to represent the hazard
98 intensity of TCs (i.e., *global* form) considering the vast area affected by TCs. On the
99 other hand, it remains unknown whether the damage function in *local* form derived
100 from TC scale applies to finer scales.
101
102 Therefore, starting from the distinction between the two types of damage function,
103 this study contributes to reaching a goal of understanding the effect of spatial scale on
104 tropical cyclone damage function and a better connection of TC economic impact
105 studies and TC risk management at different scales. The objectives of this study are to
106 (1) construct TC damage functions at different spatial scales in the forms of sigmoidal

curves and power-law-based models, (2) perform scale-dependence analysis, i.e., explore how the structure, parameters and performance of the damage function vary with spatial scale, and (3) discuss the implications in both damage function selection and risk management at different spatial scales.

2 Data and Methods

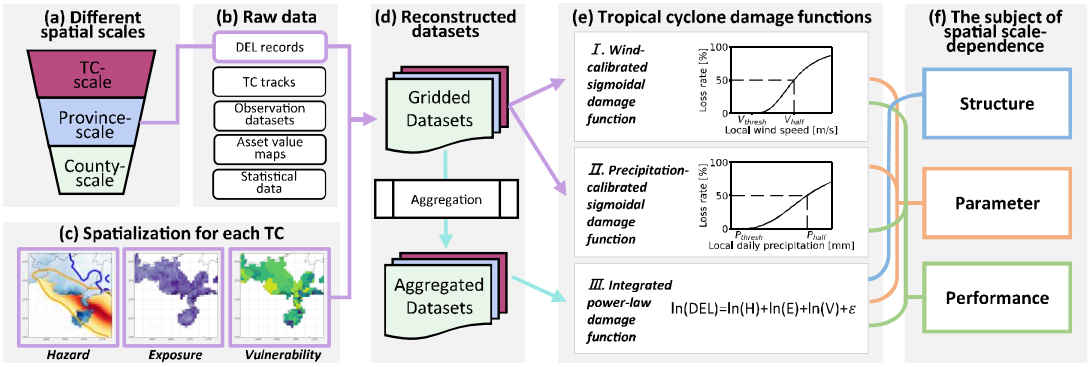

Figure 1 Schematic overview of the data and methods applied to explore the spatial scale-dependent effects of the TC damage functions over China.

To explore the spatial scale dependence of the TC damage function over China, the data preparation process and scale-dependence analysis methods are illustrated in Figure 1. First, DEL records at different spatial scales are collected. For each DEL record, its corresponding hazard distribution is simulated or extracted based on the TC track and TC lifetime (Sect. 2.1.1.1). The hazard distribution determines the geographic extent of exposure and vulnerability, and thus the spatialization of exposure and vulnerability is completed (Sect. 2.1.1.2 to Sect. 2.1.1.3). Second, these spatially explicit data, together with DEL records at three different scales, form the "gridded datasets" and "integrated datasets" (Sect. 2.1.2), which are used in the estimation and comparison of sigmoidal and power-law damage functions, respectively (Sect. 2.2.1). Finally, the spatial scale dependence is analyzed from three subjects (Sect. 2.2.2).

2.1 Data

2.1.1 Data source and preprocessing

2.1.1.1 TC damage and hazard distribution

TC damage data (i.e., DEL records) are required on different spatial scales to calibrate TC damage functions and compare their performance. We use DEL records from two sources. The first source records come from the Ministry of Emergency Management of the People's Republic of China (MEM), setting the county as the basic statistical unit and collecting DEL records of 23 TC events from 2009-2015. The second source records come from the "National Climate Impact Assessment" compiled by the National Climate Center of China Meteorological Administration (CMA, 2016), setting the province as the basic statistical unit and collecting DEL records of 157 TC events from 1990-2015. In this study, we also define the DEL records from the first source as the "short sequence" and DEL records from the second source as the "long sequence". Thus, all DEL records from the two sources are reorganized into 5 subsets with different spatial scales and sequence lengths (Figure 2). The reason for not fusing the DEL data from these two sources is that, this study is concerned with spatial scale dependence and therefore needs to ensure that the overall recorded DEL remains consistent across spatial scales. Some affected provinces did not have county-level DEL records, their damage data are only included in long sequence. The long sequences provide more reported samples on province- and TC event scale, as county-level TC damage data is not always available, the short sequences serve as a sensitivity complement in scale-dependence exploration, and the overall recorded DEL remains consistent across spatial scales. All economic values in this paper are deflated to the 2005 constant Chinese yuan (CNY). Note that the DEL data and asset value exposure are deflated by the consumer price index (CPI), and gross domestic product (GDP) values are deflated by the GDP deflator. The CPI and GDP deflator of China are available in the World Development Indicators from World Bank.

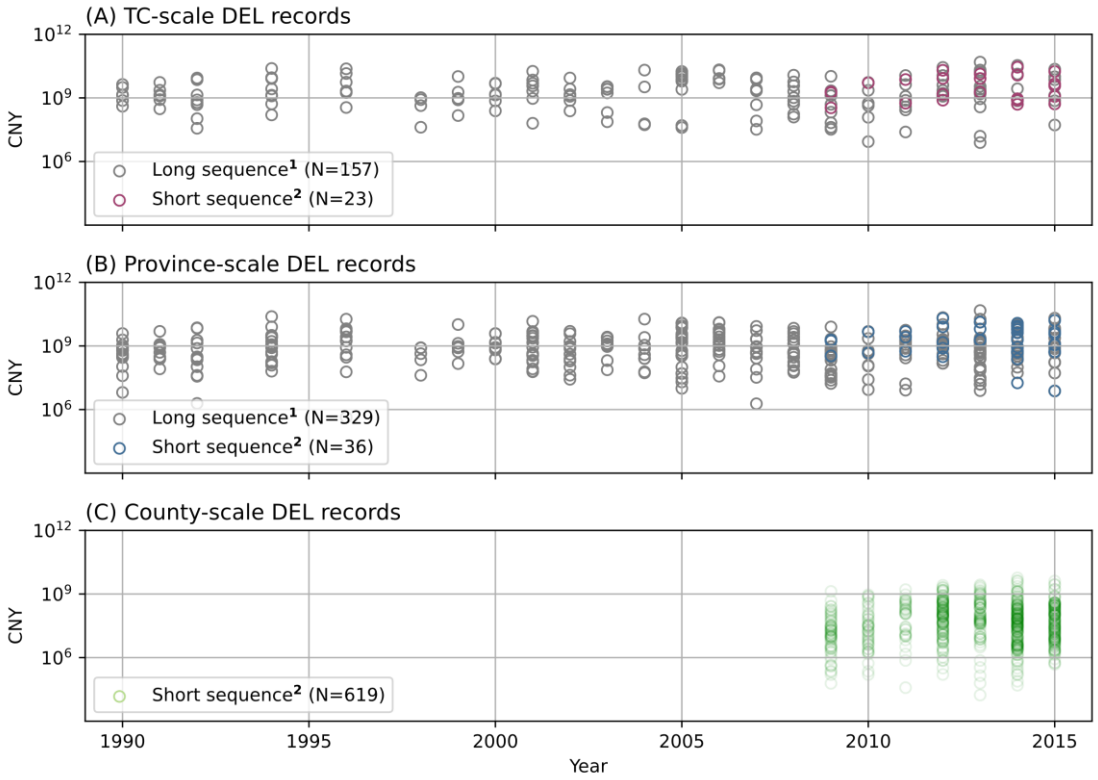

Figure 2 The DEL records with different spatial scales and sequence lengths in this study. The superscript 1 indicates that the source is CMA (2016), and the superscript 2 indicates that the source is EME.

For hazards, we consider that DEL is determined by both wind and TC-induced precipitation. Here, wind intensity is represented by wind fields, i.e., the geographic distribution of the 2 min-sustained wind speed at 10 m above ground per TC event, referred to as "wind speed" or "wind intensity" in the following sections. Wind speed is simulated at a horizontal resolution of 0.25°×0.25° from historical TC tracks as a function of time, location, the radius of maximum winds, and central and environmental pressure based on the revised hurricane pressure-wind model by Holland (2008). Historical TC tracks are obtained from the International Best Track Archive for Climate Stewardship (IBTrACS) (Knapp et al., 2010, 2018). The best track record of an individual TC includes the location of a TC every six hours from generation to extinction. The wind speeds of TCs are reported very differently by many international agencies. The wind speeds used in this study are from the CMA, and its wind speed averaging period is 2 minutes (Lu et al., 2021). Based on the

TC-scale DEL records, a total of 157 TC tracks affecting mainland China from 1990 to 2015 are selected (Figure S1). Next, we use CLIMADA v1.4.1 (Bresch & Aznar-Siguan, 2021), a free, open-source software package written in Python 3.7 and made available online on GitHub, to generate the wind field for each selected TC track. For each grid point in the area within 500 km of the TC track and with the DEL record, if the wind intensity exceeds 17.2 m/s (~33 knots), the grid is considered to be affected by tropical storm or tropical cyclone (WMO, 2015). Tropical depression grids with wind speeds less than 17.2 m/s are not included.

TC-induced precipitation intensity is represented by maximum daily precipitation during the TC lifetime. Historical precipitation can be obtained from CN05.1, which is a gridded daily scale observation dataset with a high spatial resolution of 0.25°×0.25° over China (Wu et al., 2017) and comprises several variables, including daily precipitation. CN05.1 has been widely used to analyze observed climate features over China and to evaluate the performance of global and regional models (Bucchignani et al., 2017; Sun & Wang, 2015). According to the TC lifetime information derived from IBTrACS, the maximum daily precipitation during the TC lifetime of each grid is identified. For each grid point in the area within 500 km of the TC track and with the DEL record, if the daily precipitation exceeds 25 mm, the grid is considered to be affected by TC-induced precipitation (Chen et al., 2011).

2.1.1.2 Asset value exposure

Asset value is considered a better indicator of DEL exposure than GDP for the assessment of natural hazard-induced disasters (UNISDR, 2015; Wu et al., 2019). Here, wind together with TC-induced precipitation determine the geographic extent of TC exposure and therefore the vulnerability of the exposed area. To match the hazard, exposure, and vulnerability in space, the resolution of asset value exposure and vulnerability needs to be spatialized to 0.25 degrees, which is consistent with that of CN05.1. For exposure, we generate gridded datasets of asset values based on the previous work of Wu et al. (2014; 2018), including a 30-arc-second spatial resolution

asset value map in 2015 and county-level asset value estimates from 1990 to 2015. Here, we first aggregate the 30-arc-second asset value map to 0.25 degrees, and then assume that the county-level spatial distribution of asset values from 1990 to 2015 is the same as in 2015. From this, by calculating the asset value weights for each grid within the county in 2015, combined with the county-level asset value estimates, the spatial distribution in 2015 can then be extended to other years:

$$k_{i,j,t}=K_{j,t}\times weight_{i,j,2015} \quad (1)$$

with

$$weight_{i,j,2015}=\frac{k_{i,j,2015}}{K_{j,2015}} \quad (2)$$

where $k_{i,j,t}$ is the asset value in year t at grid i in county j, $K_{j,t}$ is the county-level asset value, and $weight_{i,j,2015}$ is the ratio of grid i to total county assets in 2015.

2.1.1.3 Vulnerability

For vulnerability, we use statistical data on GDP per capita and house structure to represent the socioeconomic and physical capacity to reduce the economic impact of TCs, respectively. GDP per capita at the county level from 1990 to 2015 are collected from the Chinese Socioeconomic Development Statistical Database (CSDSD, https://data.cnki.net/). Here, we assume that the GDP per capita of each county are uniformly distributed, that is, the GDP per capita of each 0.25-degree grid are equal to that of the county where the grid is located.

House structure is described by the proportion of nonsteel-concrete residential buildings (NSCB). County-level statistics on residential buildings by different load-bearing frame structure types from population censuses are available for 2000 and 2010 in China, which also can be accessed from CSDSD. Since such census data are not available for other years, we assume that the proportion of NSCB was constant for a county from 1990 to 2015, and we use the value of 2010 to represent the proportion of NSCB for the whole period. The proportion, always between 0 and 1, indicates the ratio of relatively vulnerable housing of a county. Similarly, we assume

that the proportion is uniformly distributed within a county. Although this ratio could not provide information on temporal variation of the house structure, it introduces spatial physical vulnerability and could indicate the possibility of capital stock transformed into economic damage from the mechanism.

2.1.2 Dataset reconstruction

After preprocessing the data, we complete the spatialization of TC hazard (by simulating the wind field and extracting the precipitation field from observed data), exposure (by upscaling and extending an existing asset value map), and vulnerability (by spatializing statistical data) at 0.25 degrees. These spatially explicit data, together with DEL records at three different scales, form the "gridded datasets" that are used for calibrating the sigmoidal damage function. A total of 56,023 grid points affected by TCs are included, and each grid point has 5 properties: wind speed, daily precipitation, asset value, GDP per capita, and the proportion of nonsteel-concrete residential buildings.

Furthermore, we aggregate spatially explicit data to match DEL records at three different scales. For hazard, exposure, and vulnerability, different aggregate functions are used. We use the *max* and *average* function for wind and precipitation intensity to describe the potential maximum and mean intensity at the county, province, and TC levels, respectively. Four hazard variables, $W_{\max}$, W_{avg}, $P_{\max}$, and P_{avg}, are generated. Gridded asset value exposure (K) is aggregated using the *sum* function to show the total assets exposed by TCs. GDP per capita (I) and house structure (H) data are aggregated using the *average* function to determine the overall vulnerability of the exposed area. Finally, all aggregated variables, together with DEL records at three different scales, form the "aggregated datasets" that are used for estimating the integrated power-law damage function. More intuitively, each DEL record in Figure 2 and 7 explanatory variables matching each record exactly form the aggregated datasets (see more in Figure S2).

2.2 Scale-dependence analysis

2.2.1 Two types of damage functions

The damage function, or impact/vulnerability function, relates the TC intensity to the damage it may cause. Earlier studies tended to suggest a high power-law dependence of damage on wind speed (Howard et al., 1972; Iman et al., 2005; Nordhaus, 2006, 2010; Pielke, 2007); that is, damage induced by TCs appears to rise with the third to ninth power of maximum wind speed. Starting from Mendelsohn et al. (2012), the damage function incorporates additional determinants. For example, Mendelsohn et al. (2012) assumed that damage is represented by the intensity and location of TCs, regressing damage per TC on intensity (measured as wind speed and minimum pressure, respectively), population density, and income. Here, all dependent and independent variables are converted into logarithmic form because the log-log function form is the best fit, as affirmed by various studies (Bakkensen & Mendelsohn, 2016; Geiger et al., 2016). Therefore, the estimated coefficient of wind speed in the regression is the nth power of wind speed from previous studies. The US coefficient on wind speed is 4.95 (with a standard error of 0.63), revealing that damage varies as the nearly fifth power of wind speed or a 20% increase in wind speed would double the damage (Mendelsohn et al., 2012). However, TC winds are commonly accompanied by intense precipitation, which can also cause significant damage. Bekkensen et al. (2018) performed a TC integrated damage assessment at the province scale with two characterizations, namely, wind + rain and wind-only, where the former damage function includes both wind and rain as explanatory variables while the latter includes only wind.

In contrast to studies that attribute losses to maximum wind speed at the province or TC scale level, another strand of studies is devoted to characterizing the damage function that can describe the relationship between local wind speed and loss ratio. Emanuel (2011) proposed a damage function that produces positive values of damage only for wind speed over a specified threshold, and the mean damage ratio should vary as the cube of the wind speed over the threshold, and then the ratio approaches

100% at very high wind speed. An idealized sigmoidal damage function that satisfies these requirements is

$$LR=\frac{V_{\mathrm{n}}^{3}}{1+V_{\mathrm{n}}^{3}} \tag{3}$$

with

$$v_{\mathrm{n}}=\frac{\mathrm{MAX}[(V-V_{\mathrm{thresh}}),0]}{V_{\mathrm{half}}-V_{\mathrm{thresh}}} \tag{4}$$

Equation (3) defines the loss rate LR as a function of wind speed (V). Fundamentally, LR is determined by two shape parameters, V_{thresh} and V_{half}. By varying the two parameters, the damage function can be fit to describe the vulnerability of various building types (Sealy & Strobl, 2017) or different countries and regions (Eberenz et al., 2021).

In this study, the above two types of damage functions, i.e., the sigmoidal curve-based damage function and power-law damage function, are separately used to model the DEL from TCs in China at the county, province, and TC scales. Previous sigmoidal curve-based damage functions only consider the effect of wind intensity on damage, and its form is given in Equations 3 and 4, hereinafter referred to as the "wind-calibrated sigmoidal damage function". In the same form, but using TC precipitation to represent the hazard, we propose a new TC damage function referred to as the "precipitation-calibrated sigmoidal damage function", i.e., the loss rate LR is defined as a function of daily precipitation (P) and determined by two shape parameters, P_{thresh} and P_{half} (see Equations 5 and 6).

$$LR=\frac{P_{\mathrm{n}}^{3}}{1+P_{\mathrm{n}}^{3}} \tag{5}$$

$$P_{\mathrm{n}}=\frac{\mathrm{MAX}[(P-P_{\mathrm{thresh}}),0]}{P_{\mathrm{half}}-P_{\mathrm{thresh}}} \tag{6}$$

For the power-law damage function, we consider an integrated model with all three components (i.e., hazard, exposure, and vulnerability) introduced. The integrated model predicts the DEL given the explanatory variables from three components. We refer to it as the "integrated power-law damage function", and the full equation is

$$\ln(\mathrm{DEL})=\beta_0+\beta_H\ln(H)+\beta_E\ln(E)+\beta_V\ln(V) \tag{7}$$

where *H, E, and V* are hazard, exposure, and vulnerability variables, respectively.

These two types of damage functions correspond to the two datasets reconstructed above. The sigmoidal damage functions convert the wind or precipitation intensity at each 0.25-degree grid point into a certain loss rate using the gridded datasets for parameter calibration and performance comparison. However, the integrated power-law damage function directly relates the DEL at the county, province, or TC scale to hazard, exposure, and vulnerability variables at the same spatial scale, using the aggregated datasets for parameter estimation. To compare the ability to reproduce the DEL under different damage functions and different spatial scales, the record damage ratio (RDR) is computed for each record R as the ratio of the simulated DEL over the reported DEL (Eberenz et al., 2021):

$$\mathrm{RDR}_R = \text{Simulated DEL}_R / \text{Reported DEL}_R. \quad (8)$$

If a RDR equals 1, it indicates a perfect fit between its corresponding simulated and reported DEL. A RDR greater than 1 indicates an overestimation of DEL; otherwise, an underestimation. In addition, to compare the ability to reproduce the total DEL under a certain spatial scale, the total damage ratio (TDR) is calculated as the sum of the simulated DEL divided by the sum of the reported DEL:

$$\mathrm{TDR}_S = \frac{\sum_{R=1}^{N} \text{Simulated DEL}_R}{\sum_{R=1}^{N} \text{Reported DEL}_R} \quad (9)$$

where N is the number of DEL records R in subset S. Notably, records with a large DEL will have a significant impact on the value of the TDR.

2.2.2 The subject of spatial scale dependence

We follow the subject of spatial scale dependence proposed by Sandel (2015), i.e., TC damage functions are scale dependent when the model structure, estimated parameters or model performance varies with spatial scale.

First, the scale-dependence of structure only occurs when the multiple variables included in a damage function vary with spatial scale or sequence length. Thus, we use an integrated power-law damage function to perform the scale-dependence of the

structure. Specifically, variable selection analysis is performed to illustrate how the variables selected to be included in an integrated damage function vary with spatial scale. Considering the integrity of the risk framework, at least one explanatory variable should be kept for each component of hazard, exposure, and vulnerability. Here, we use the root-mean-squared fraction (RMSF) as a cost function following Eberenz et al. (2021) to pick the optimal structure of the damage function:

$$\mathrm{RMSF}=\exp\left(\sqrt{\frac{1}{N}\sum_{R=1}^{N}\left[\ln(\mathrm{RDR}_R)\right]^2}\right). \quad (10)$$

The RMSF is a measure of the spread in RDRs. The larger the relative deviation between the simulated and reported DEL for all records is, the larger the value of the RMSF. The most ideal value of the RMSF for a perfect fit of all records is 1. Therefore, we can obtain the optimal structure of the damage function by identifying the function associated with the smallest value of RMSF; see Sect. 3.1 for the results.

Second, we use both types of damage functions to illustrate the scale dependence of the parameter. For two damage functions in sigmoidal form, similar parameter calibration procedures are adopted. In a function using the intensity of wind to represent hazard, the threshold wind speed V_{thresh} is set as 25.7 m/s, which was first proposed for the USA by Emanuel (2011) and then affirmed for China by Elliott et al. (2015). When V_{thresh} is identified, V_{half} becomes the only parameter that determines the slope of a sigmoidal function. For the fitting of V_{half}, we use the RMSF again to find the optimal value of V_{half} under each spatial scale, i.e., the optimized V_{half} associated with optimal results for each cost function is identified. Thus, the value of optimized V_{half} is the parameter of the wind-calibrated sigmoidal damage function. In a function using the intensity of TC precipitation to represent hazard, the threshold daily precipitation intensity P_{thresh} is set as 25 mm (Chen et al., 2011; Ye et al., 2020). Adopting the same calibration procedure, the P_{half} associated with the optimal value of the RMSF is the parameter of the precipitation-calibrated sigmoidal damage function. For the integrated damage function in power-law form, parameters are estimated in the same structure to exclude the influence of explanatory variable

selection. That is, the natural log of DEL is a function of maximum wind intensity ($W_{\max}$), maximum precipitation intensity ($P_{\max}$), asset value exposed to TC (K), and GDP per capita (I). We select this functional form in line with previous literature (Bakkensen et al., 2018; Mendelsohn et al., 2012; Ye et al., 2020) and improve it in three ways: 1) the DEL is codetermined by hazard, exposure, and vulnerability; 2) in addition to wind, TC-induced precipitation is introduced to indicate hazard; and 3) the asset value instead of GDP exposed by TCs is introduced to represent exposure. Thus, $\beta_{W_{\max}}$, $\beta_{P_{\max}}$, β_K, and β_I are parameters of the integrated power-law damage function. The values of these parameters at different spatial scales are used to demonstrate the scale-dependent effect of the parameter (Sect. 3.2) and to compute the RDR for each record and the TDR for each subset, allowing for the comparison of model performance in Sect. 3.3.

Finally, after parameter estimation, the scale dependence of performance can be analyzed; considering the fact that, on the one hand, the number of current DEL records must be much smaller than the total number of TC events causing damage, on the other hand, most previous studies have estimated DEL at the TC scale. Therefore, the scale dependence of performance is illustrated in two ways. One is how the performance changes when using parameters derived from a short sequence to evaluate DEL at a long sequence (Figure 6). Another is how the performance changes when using parameters derived from the TC scale to evaluate DEL at a finer scale (Figure 7).

3 Results

3.1 Scale dependence of the structure

In this section, the integrated power-law damage function (Equation 7) is used to demonstrate how spatial scale and sequence length affect the structure of the TC damage functions. Table 1 lists the optimal combination of explanatory variables in

each case. For short sequences, the wind variable (i.e., W_{max}) is always the most significant. Precipitation variables (i.e., P_{max} and P_{avg}) are not always important, but their importance decreases as the spatial scale increases. In contrast, the significance of exposure variable K increases as the spatial scale increases. Similarly, for long sequences, the importance of the exposure variable increases with spatial scale, while the relative importance of hazard variables decreases with scale (though they are consistently significant at the 0.001 level). Unlike the short-sequence results, the wind variable is relatively less important than the precipitation variable. Comparing the selected variables on the same spatial scale but with different sequence lengths, an identical pattern is that the relative significance of the wind variable decreases with sequence length, but the relative significance of the precipitation variable increases with sequence length. In addition, the choice of two different vulnerability variables (i.e., physical vulnerability H and social vulnerability I) varies with the spatial scale and sequence length, but the pattern does not seem to be fixed.

Table 1

Variable selection results by spatial scale and sequence length

Sequence Length	Short Sequence			Long Sequence	
Spatial Scale	County	Province	TC	Province	TC
1	W_{max}^{***}	W_{max}^{***}	W_{max}^{***}	P_{max}^{***}	K^{***}
2	P_{max}^{***}	P_{max}^{*}	K^{**}	W_{max}^{***}	P_{max}^{***}
3	I^{***}	K^{*}	H	H^{***}	W_{max}^{***}
4	K	I	P_{avg}	K^{**}	I^{***}
RMSF	5.6	2.1	1.8	4.1	3.6
R^2	0.389	0.818	0.789	0.405	0.569

Note. Selected variables are listed in the order of statistical significance. ***, **, and * indicate significance at the 0.001, 0.01, and 0.05 levels, respectively. The specific estimated coefficients are shown in Table S1.

The partial regression plots more intuitively explain why the integrated power-law damage function has this structural scale dependence. Increasing the spatial scale, the

partial regression coefficient of precipitation variable $P_{\max}$ becomes more negative (Figure 3b, Figure 3e), while the partial regression coefficient of exposure variable K becomes more positive (Figure 3c, Figure 3f) for both short and long sequences. That is, as the spatial scale increases, asset exposure tends to more significantly determine the amount of DEL, while the role of precipitation intensity is not as significant as it is for smaller scales. Less variation in the partial regression coefficient of wind variable $W_{\max}$ at different spatial scales is observed, especially for the long-sequence case (Figure 3d). Combining the results of selected variables and partial regression plots on wind, precipitation, and exposure variables, it is suggested that 1) the *global* wind intensity is statistically associated with DEL at all spatial scales, and such a relationship tends to be consistent across spatial scales as the sequence is prolonged; 2) the contributions of *global* precipitation intensity and total asset exposure to DEL are spatial scale dependent in the structure of the power-law TC damage function; and 3) the choice of vulnerability indicator is spatial scale dependent.

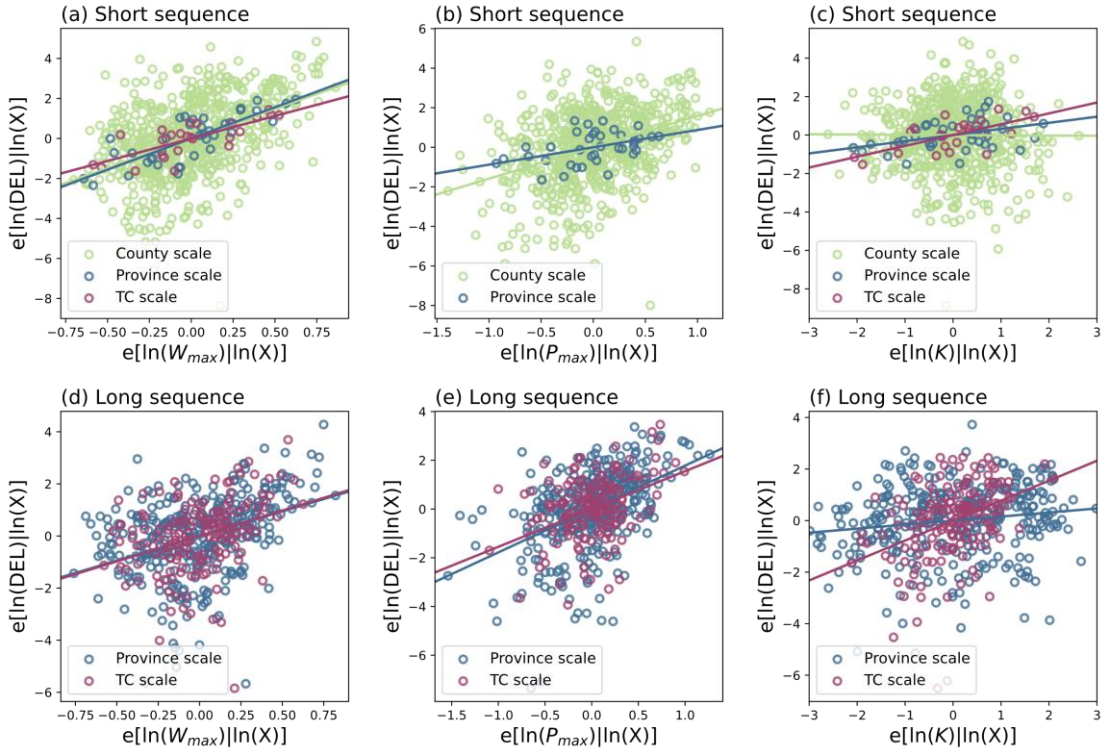

Figure 3 The partial regression plots based on the explanatory variables selected in Table 1.

443

444 **3.2 Scale dependence of the parameter**

445 In this section, the sigmoidal damage function based on wind (Equation 3 and
446 Equation 4) and precipitation (Equation 5 and Equation 6) and the integrated
447 power-law damage function (Equation 7) are used to demonstrate how the spatial
448 scale and sequence length affect the parameter of the TC damage functions. Figure 4
449 represent the parameter comparison in sigmoidal form, using local maximum wind
450 speed daily precipitation as indicators of hazard intensity, respectively. In addition to
451 comparing the best fit of slope parameter V_{half} (P_{half}) to simulate the DEL at county,
452 province, and TC scales (Figure 4a, b), the individually fitted values of V_{half} (P_{half})
453 for each DEL record are given to visualize the uncertainty in each subset (Figure 4c,
454 d).

455

456 For the short sequence, the calibrated V_{half} at the county, province, and TC scales is
457 62.4, 60.9, and 52.9 m/s, respectively. For the long sequence, the calibrated V_{half} at
458 the province and TC scales is 40.8 and 48.2 m/s, respectively. Comparing the position
459 of calibrated V_{half} and the interquartile range (IQR) containing 50% of the
460 individually fitted DEL records, the former tends to be located at a very left position
461 within the IQR, or even smaller than the IQR (Figure 4c). It is indicated that the
462 calibrated optimal V_{half} using local wind intensity is still unable to accurately
463 describe the real damage function. This will be further analyzed and discussed in Sect.
464 3.3 and Sect. 4.1. Conversely, the calibrated sigmoidal damage function based on
465 local daily precipitation seems to be more ideal in interpreting each DEL sample since
466 all calibrated P_{half} are located within the corresponding IQR (Figure 4d), and the
467 median values are very close to calibrated P_{half}, especially for the long-sequence case.
468 For the short sequence, the calibrated P_{half} at the county, province, and TC scales is
469 560, 528, and 624 mm, respectively. For the long sequence, the calibrated P_{half} at the
470 province and TC scales is 449 and 510 mm, respectively. It should be noted that the
471 median of the individually fitted P_{half} increases with the spatial scale, which is in line

with expectations. However, comparing the values of calibrated P_{half} as the spatial scale increases, the case of province scale and short sequence breaks the rule. The value of 528 mm is the smallest for the short sequence, and it deviates the most from the median. This anomaly reveals the uncertainty of short sequences for calibration parameters. Another interesting fact is that prolonging the sequence length would lead to a smaller value of P_{half}, which is confirmed both at the TC and province scales. This can be explained by the fact that the long sequence contains more small loss rate (*LR*) records (for long and short sequences, the median *LR* at the province scale is 0.11% and 0.17%, and the median *LR* at the TC scale is 0.13% and 0.21%, respectively), since large damages are always rare. In general, the slope parameter P_{half} is spatially scale dependent, as it tends to become larger with increasing scale, although it is more robust for long sequences.

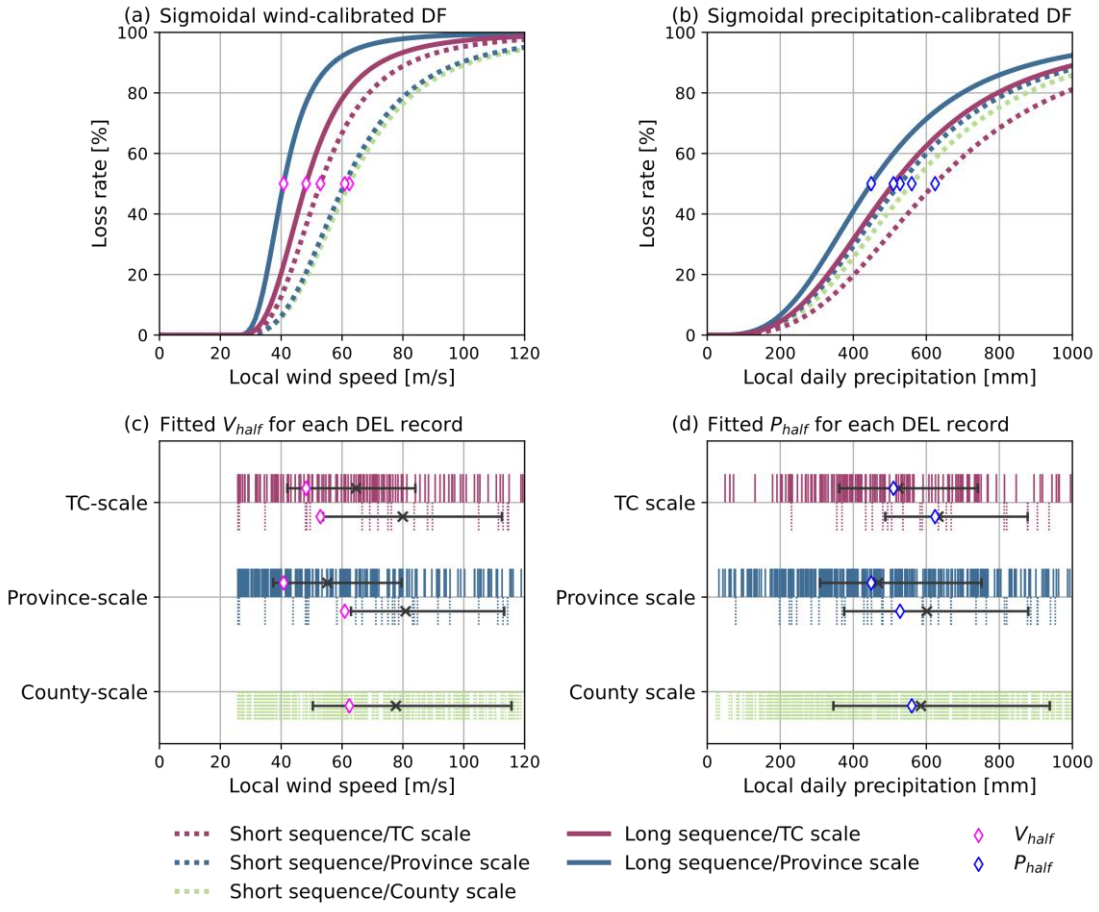

Figure 4 Calibrated results of sigmoidal damage function (DF) based on local wind **(a)** and precipitation **(b)** intensity for different spatial scales. The individually fitted

values of V_{half} **(c)** and P_{half} **(d)** for each DEL record are shown in vertical lines, and their interquartile range and median in each subset are shown in black horizontal line segments and crosses, respectively. The fuchsia (blue) diamonds mark the position of V_{half} (P_{half}) at different spatial scales.

Instead of using *local* hazard intensity, the integrated power-law damage function using *global* hazard intensity also shows the scale dependence of the parameter. Taking the model structure proposed in Sect. 2.2.2 as an example, i.e., hazard is represented by *global* maximum wind intensity ($W_{\max}$) and maximum daily precipitation ($P_{\max}$), exposure is represented by asset exposure (K) and vulnerability is represented by GDP per capita (I). Figure 5 demonstrates the estimated regression coefficients varying with spatial scale and sequence length. For each case, the coefficient of $W_{\max}$ is always significantly larger than zero, although it deviates from zero by different degrees. The coefficients of the other three explanatory variables can all be insignificant at certain spatial scales. Such parameter dependence is consistent with the structure-dependence results shown. For example, $W_{\max}$ is always introduced as an explanatory variable in the optimal structure under each spatial scale and is statistically significant in Table 1. The coefficients of $P_{\max}$ exhibit a more regular spatial scale dependence. Its value decreases with spatial scale, accompanied by a decrease in confidence (Figure 5b), which is consistent with the fact that its relative importance ranking decreases with scale (Table 1). The coefficient of K is not significantly different from zero at the county scale but is significant at the province and TC scales, especially for long sequences. This mutually corroborates the partial regression plots in Figure 3c and Figure 3f. In addition, it should be noted that the coefficient of I at the county scale is 0.58 and is positively significant. Given that the coefficient of K at the county scale is not significantly different from zero, GDP per capita represents exposure rather than expected social vulnerability. The case where all introduced explanatory variables are statistically significant is only shown at the TC scale for long sequences. The estimated coefficients, also called elasticity in such log-log relationships, of $W_{\max}$, $P_{\max}$, K and I are 1.95 [1.07 to 2.83, 95% confidence interval], 1.55 [0.93 to 2.20], 0.77 [0.48 to 1.07], and -1.14 [-1.77 to -0.51] ,

519 respectively, indicating that a doubling of *global* maximum wind speed, *global* daily
520 precipitation, asset exposure, and GDP per capita increase the TC scale's DEL by 286%
521 [110% to 611%], 193% [90% to 359%], 71% [39% to 110%], and -55% [-71% to
522 -30%], respectively. Particularly, the coefficient of I is negatively significant,
523 demonstrating that the impact of socioeconomic vulnerability on mitigating DEL,
524 proxied by GDP per capita, is revealed for TC-scale and long-term estimation. The
525 estimated elasticities of maximum wind speed are much smaller than the previous
526 damage functions that did not consider the effect of TC-precipitation(Mendelsohn et
527 al., 2012; Nordhaus, 2010). Our results show that DEL rises with less than third power
528 of the maximum wind speed at the 95% confidence level, thus the higher power-law
529 dependences of damage on wind speed overestimate the effect of wind.
530

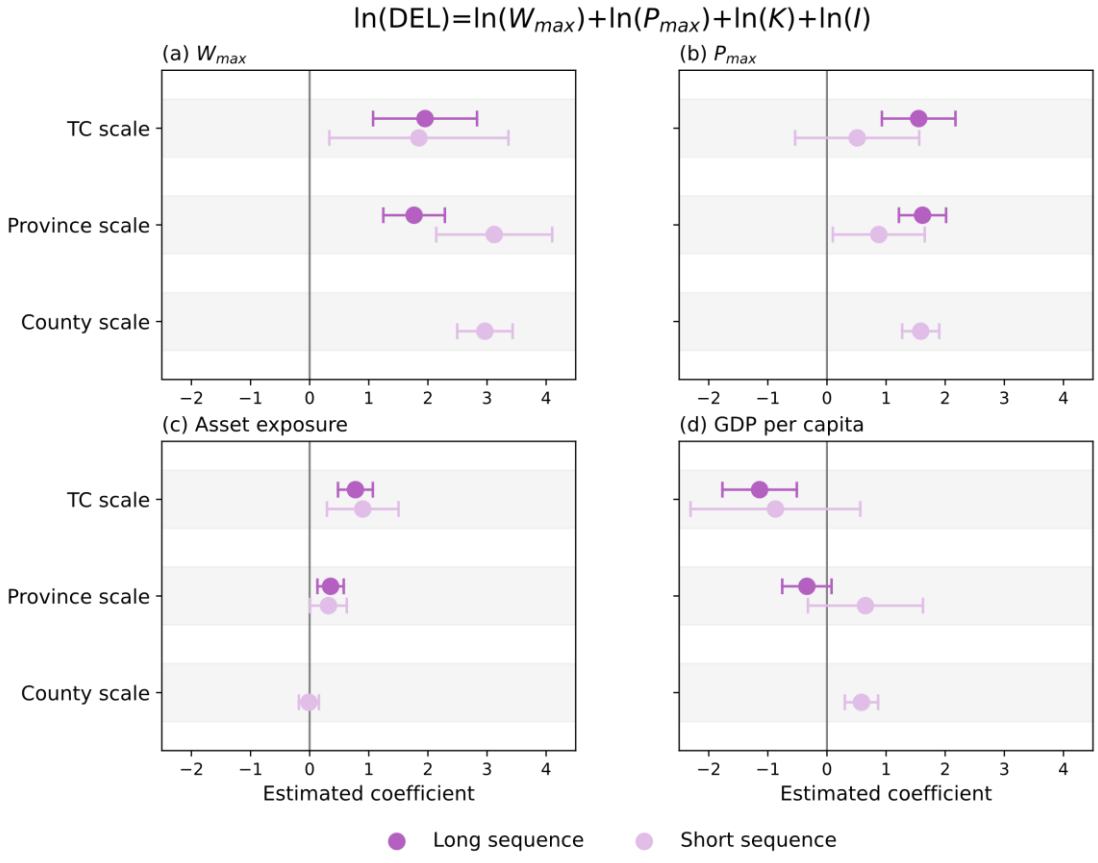

531

532 **Figure 5** Regression coefficient of the integrated power-law damage function using
533 *global* hazard intensity varying with spatial scale and sequence length. The
534 explanatory variables used here are based on the selection in Sect. 2.2.2. The error
535 bars show the 95% confidence interval of the coefficient.

3.3 Scale dependence of the performance

In this section, the three damage functions that were parameterized in Sect 3.2: (1) sigmoidal damage function based on local wind and (2) precipitation intensity, and (3) integrated power-law damage function, are used to demonstrate how spatial scale and sequence length affect the performance. In scenarios using parameters derived from short sequences (SSs) to evaluate DEL at long sequences (LSs), the performance comparison by three damage functions is shown in Figure 6. In scenarios using parameters derived from the TC scale (TCS) to evaluate DEL at a finer scale, the performance comparison by three damage functions is shown in Figure 7.

Obviously, the difference in performance brought by different damage functions is greater than the difference due to the inconsistent sequence length. Among the three functions we use, it is clear that the overall performance of the wind-calibrated damage function is the least ideal, both in terms of the spread of deviation of the individually simulated DEL from the reported DEL and the ratio of the total simulated DEL to the total reported DEL (Figure 6a). It is associated with the biasedly calibrated V_{half} in Figure 4. Calibrating the sigmoidal TC damage function with the wind field is not capable of adequately modeling the economic cost of TCs. The consequence of using the wind-calibrated damage function is that an impractically low value of V_{half} is obtained, and this is a kind of compensation for the fact that the wind field is not enough to represent TC hazard. Therefore, the highly simulated DEL for individual records and high TDR for all records are shown. The absence of the minimum and lower quartiles of the RDR at the province scale and long sequence is because approximately a quarter of the simulated DELs are equal to 0. This also illustrates the limitation of the wind-calibrated damage function, as the reported DEL actually exists, and the wind-calibrated damage function fails to reproduce it. It is further visualized in the case of TC Morakot and TC Lisa (Figure 8). The precipitation-calibrated and integrated power-law damage functions indicate better simulation results in regard to the RDR, but the former shows an overall overestimation in TDR (Figure 6b), and the

latter underestimates (Figure 6c). In the same form of damage function, the short sequence shows relatively better estimates of DEL due to its lower heterogeneity than the long sequence. In scenarios using parameters derived from SSs to evaluate DEL at LSs, worse performance is shown in the RDR, while better performance is shown in the TDR. For relative larger scales like province- and TC-scale, short sequence may be adequate to describe a robust relationship in both forms of damage function.

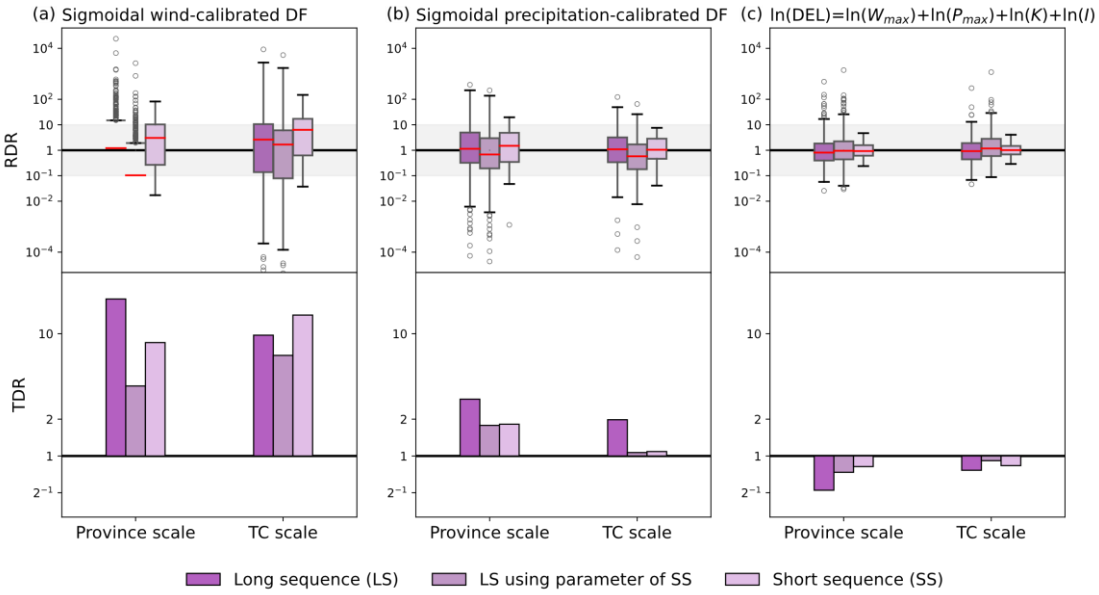

Figure 6 Performance comparison of three damage functions (DFs) using parameters derived from short sequences to evaluate DEL at long sequences. **(a)** Sigmoidal DF based on local wind and **(b)** precipitation intensity, and **(c)** integrated power-law DF. Performance is represented by a boxplot of the RDR (i.e., the deviation of the individually simulated DEL from the reported DEL) and the TDR (i.e., the ratio of total simulated DEL to total reported DEL), respectively.

Similarly, the difference brought by different damage functions is greater than the difference due to the inconsistent spatial scale. Here, we concentrate on precipitation-calibrated and integrated power-law damage functions for their better performance. First, for both types, the spread of the RDR at the TC scale is less variable than at the province/county scale for its minimum IQR. These results are consistent with the regularity presented by sequence length, i.e., a larger spatial scale and shorter sequence usually indicate a smaller sample size and thus reduce the intrasample heterogeneity, which is finally indicated as a smaller IQR in the boxplot.

Second, in terms of the TDR, the performance also improves with spatial scale. Except for the short-sequence case in Figure 7b, the value of the TDR at the province scale is higher than that at the county or TC scale. This result is consistent with the smallest value of P_{half} for the province scale in Figure 4b. Again, the two types of damage function show opposite directions in the TDR. Combining the performance of the RDR and TDR, the precipitation-calibrated damage function in sigmoidal form is suitable for county-scale simulation, only biasing the TDR by a factor of less than 2. The power-law damage function is more effective at the province and TC scales. For most records, the simulated DEL and reported DEL deviate by less than 1 order of magnitude. However, when scaling the parameter of the TC scale to finer scales, the performance of sigmoidal precipitation-calibrated damage function at TC scale shows a worse simulation than its original results, which indicate a worse scalability compared with the power-law form. Thus, for such a sigmoidal form, it is particularly important to establish a spatial scale-specific damage function.

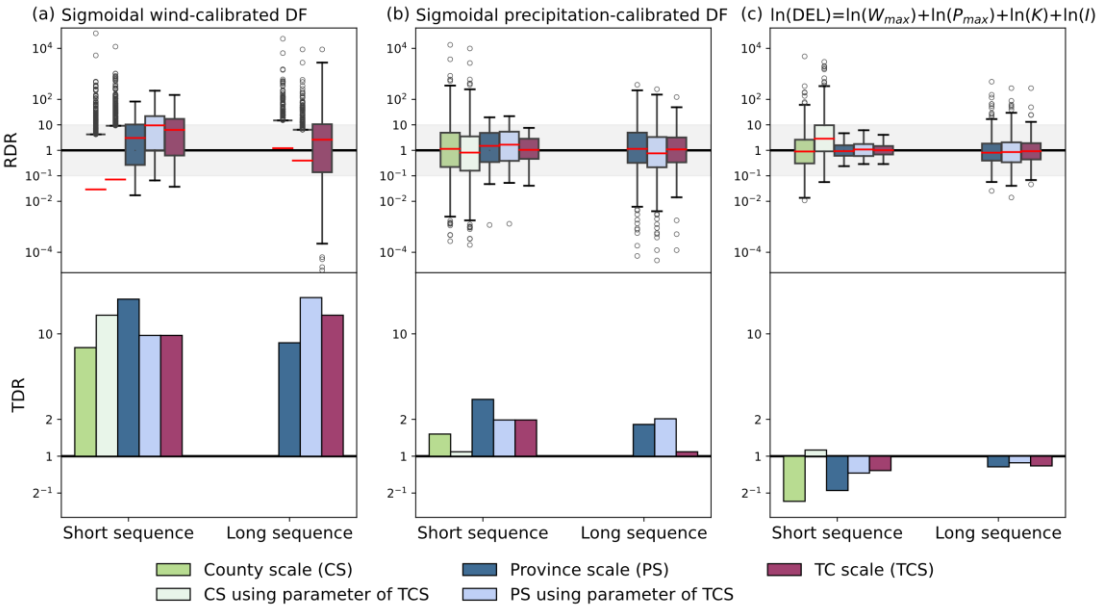

Figure 7 Performance comparison of three damage functions (DFs) using parameters derived from the TC scale to evaluate DEL at the province-/county scale. Consistent with Figure 6, performance is represented by a boxplot of RDR and TDR, respectively.

4 Discussion

4.1 Implications in TC risk management at different scales

Generally, TC risk assessment is adopted from a global or national perspective. However, the DEL records with better resolution and details at subnational levels make TC risk assessment at a finer scale feasible. Our results provide a considerable reference for TC risk management at different scales.

First, the type selection of the damage function should be spatially scale adaptive. For TC or province scales, it is more appropriate to use an integrated power-law damage function to perform TC risk assessments. A potential problem is that this may lead to a conservative assessment of future risk, given its underestimation of the TDR. At the county scale, it is advisable to employ the more scale-independent, precipitation-calibrated sigmoidal damage function. The consequent challenge is that there is much difficulty and uncertainty in predicting the spatial distribution of future exposure.

Second, TC-induced precipitation tends to be more significant in determining exposure and therefore the economic cost of TCs. This is confirmed by the parameters and performances of the two separately calibrated sigmoidal functions. The hidden reason is that a grid with a maximum wind speed lower than V_{thresh}, i.e., 25.7 m/s, may be hit by heavy rainfall and suffer significant DEL as a result. Thus, wind-calibrated sigmoidal damage functions would fail in evaluating DEL for these regions. In our DEL records, Morakot in 2003 and Lisa in 1996 caused large damages of 2.4 and 1.6 billion CNY, respectively, to Fujian Province (Figure 8). The wind intensity on land was basically below 20 m/s, while the maximum daily precipitation reached 208 and 106 mm, respectively. Thus, while the wind and precipitation intensity are correlated in most cases, the sigmoidal damage function calibrated relying only on wind may lead to significant bias. This bias is mainly due to the underestimation of exposure by omitting the areas actually affected by TC-induced

637 precipitation. As a result, the steeper sigmoidal damage functions compared with the
638 real case are calibrated because of the overestimated damage rate. We find that the
639 TDRs in Figure 7e are overestimated, which again demonstrates that characterizing
640 DEL by wind alone may lead to a misestimation. Additionally, based on the sigmoidal
641 form, damage functions calibrated by precipitation alone have a better performance
642 instead. It can be interpreted that the geographic extent of TC exposure is mainly
643 determined by the intensity of precipitation rather than wind.
644
645 Third, spatial heterogeneity determines the driving force of DEL at different scales,
646 thus providing some novel insights for TC risk management and climate adaptation
647 strategies. Within a relatively limited county region, the precise spatialization of asset
648 value exposure is vital. The sigmoidal damage function, which is considered to be
649 suitable for the county scale, inherently depends on accurate exposure data to
650 determine the amount of DEL. That is, for county-level risk assessment, a precise
651 knowledge of the spatial distribution of fixed assets may be more decisive than
652 previous perceptions. At the province scale, the role of physical vulnerability in
653 mitigating and adapting TCs is highlighted for long sequences. This is particularly
654 illuminating for provinces with potential increases in TC frequency under climate
655 change. Considering the long-term TC risk, these provincial decision-makers can
656 place a higher priority on some hard defenses. For TC scales, the coefficients of
657 hazard, exposure, and vulnerability variables are all significant, suggesting the need
658 for multidimensional risk management. Notably, the coefficient of GDP per capita is
659 significantly negative, implying that reducing socioeconomic vulnerability is an
660 effective way to mitigate the impact of TCs. From the supply–demand relationship
661 perspective, increases in income increase the demand for safety and therefore enable
662 individuals to employ costly precautionary engineering and nonengineering measures
663 (Wu et al., 2018). Consequently, the trade-off between the increase in resilience
664 against TCs and exposure brought by development is a challenging choice in regard to
665 socioeconomic pathway for national policy-makers.

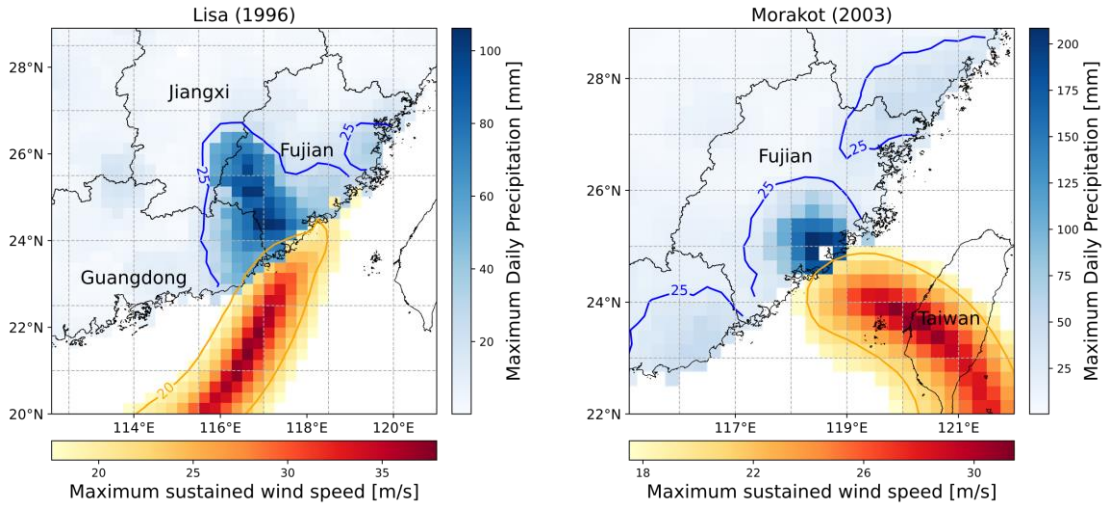

Figure 8 The wind and precipitation fields of TC Morakot in 2003 and TC Lisa in 1996. The blue lines are contours of maximum daily precipitation of 25 mm. The orange lines are contours of the maximum wind speed of 20 m/s.

4.2 Limitations

There are some limitations in our study. First, our spatial resolution of hazard, exposure, and vulnerability of 0.25 degrees may be coarse for county-level estimation. This may primarily affect the accuracy of county-level exposure, resulting in an over- or underestimation of the actual loss rate. Second, the hazard is represented by wind fields modeled from TC track data and precipitation fields reconstructed from the observation dataset. The vulnerability is represented by the spatiotemporally heterogeneous GDP per capita and the spatially heterogeneous proportion of nonsteel-concrete residential buildings. We did not explicitly quantify the uncertainties from the two representations of hazards and did not include extra indicators to describe TC vulnerability. Rather, the robustness of our results was confirmed based on the full exploration of the most pervasive hazard and vulnerability data and fine DEL records in China.

5 Conclusion

Based on historical reported DEL at the county, province, and TC scales across mainland China, we first reproduce the hazard, exposure, and vulnerability based on each record. To distinguish between different types of damage functions, we

summarize two forms: a sigmoidal form that simulates damage by identifying the loss rate of each grid point and a power-law form that estimates damage by identifying the statistical relationship between hazard, exposure, and vulnerability. In the former form, in addition to identifying the loss rate by wind intensity, we inventively use the TC-induced precipitation field to represent hazards and determine the geographic extent of exposure and vulnerability. We further parameterize and then compare the two types of TC damage functions at different spatial scales. Detailed spatial scale-dependence analysis is illustrated in three subjects: model structure, calibrated or estimated parameters, and model performance. Except for the first subject, all three damage functions are used to demonstrate the effect of spatial scale on model parameter and performance. Additional comparison is also performed between short and long sequences, as a sensitivity complement in scale-dependence exploration. Overall, the spatial scale dependence of the sigmoidal damage function is mainly reflected in the difference in the calibrated value of P_{half} (V_{half}) and the real hazard intensity at which the relative impact reaches 50% of the asset exposure. The scale dependence of the power-law damage function is mainly reflected in the different driving forces of DEL at different spatial scales.

The correlations between spatial scale, functional form, representation of hazard, and the applicability of a TC damage function challenge our understanding of disaster risk mitigation and adaptation. Based on our findings, we suggest that different TC risk assessment methods and climate adaptation strategies should be adopted at different spatial scales. For the smaller county scale, the use of a precipitation-calibrated sigmoidal damage function and concerns about current and future exposure are significant. For the larger province and TC scales, an integrated power-law damage function could provide a better fit of DEL and could improve the risk assessment for annual average loss per county or province. Furthermore, the possible strategic direction of reducing vulnerability also varies with spatial scale. It is practical for developing provinces to increase investment in hard defenses to improve physical vulnerability. From the perspective of the whole country, comprehensive measures,

718 including zoning regulations, early warning systems and emergency response systems,
719 are required to enhance socioeconomic vulnerability.
720

721 **Acknowledgments**

722 This research was supported by the National Key Research and Development Program
723 (2016YFA0602403, 2017YFC1503000), and the National Natural Science Foundation
724 of China (42077437).
725

726 **Data Availability Statement**

727 The historical TC tracks data are available in International Best Track Archive for
728 Climate Stewardship (http://ibtracs.unca.edu/). The gridded daily scale observation
729 dataset over China, CN05.1, can be downloaded by contact (wangjun@mail.iap.ac.cn,
730 see more at http://ccrc.iap.ac.cn/resource/detail?id=228). The 30-arc-second spatial
731 resolution asset value map of China in 2015 can be obtained by contact
732 (wujidong@bnu.edu.cn). The GDP per capita at the county level from 1990 to 2015
733 are collected from the Chinese Socioeconomic Development Statistical Database
734 (https://data.cnki.net/). The County-level statistics on residential buildings by different
735 load-bearing frame structure types from population censuses are also collected from
736 Chinese Socioeconomic Development Statistical Database. The CPI and GDP deflator
737 of China are available in the World Development Indicators from World Bank
738 (https://datacatalog.worldbank.org/search/dataset/0037712).
739

740 **Software Availability Statement**

741 The CLIMADA v1.4.1 is available at
742 https://github.com/CLIMADA-project/climada_python.

References

Bakkensen, L. A., & Mendelsohn, R. O. (2016). Risk and Adaptation: Evidence from Global Hurricane Damages and Fatalities. *Journal of the Association of Environmental and Resource Economists*, *3*(3), 555–587. https://doi.org/10.1086/685908

Bakkensen, L. A., Park, D.-S. R., & Sarkar, R. S. R. (2018). Climate costs of tropical cyclone losses also depend on rain. *Environmental Research Letters*, *13*(7), 074034. https://doi.org/10.1088/1748-9326/aad056

Bhatia, K., Vecchi, G., Murakami, H., Underwood, S., & Kossin, J. (2018). Projected Response of Tropical Cyclone Intensity and Intensification in a Global Climate Model. *Journal of Climate*, *31*(20), 8281–8303. https://doi.org/10.1175/JCLI-D-17-0898.1

Bresch, D. N., & Aznar-Siguan, G. (2021). CLIMADA v1.4.1: towards a globally consistent adaptation options appraisal tool. *Geoscientific Model Development*, *14*(1), 351–363. https://doi.org/10.5194/gmd-14-351-2021

Bucchignani, E., Zollo, A. L., Cattaneo, L., Montesarchio, M., & Mercogliano, P. (2017). Extreme weather events over China: assessment of COSMO-CLM simulations and future scenarios. *International Journal of Climatology*, *37*(3), 1578–1594. https://doi.org/10.1002/joc.4798

Chen, H. Y., Yan, L. N., Lou, W. P., Xu, H., & Yang, S. (2011). On assessment indexes of the strength of comprehensive impacts of tropical cyclone disaster-causing factors. *Journal of Tropical Meteorology*, *27*, 139–144. https://doi.org/10.3969/j.issn.1004-4965.2011.01.017

CMA (China Meteorological Administration). (2016). *China Climate Impact Assessment*. Beijing: China Meteorological Press.

Eberenz, S., Lüthi, S., & Bresch, D. N. (2021). Regional tropical cyclone impact functions for globally consistent risk assessments. *Natural Hazards and Earth System Sciences*, *21*(1), 393–415. https://doi.org/10.5194/nhess-21-393-2021

Elliott, R. J. R., Strobl, E., & Sun, P. (2015). The local impact of typhoons on

772 economic activity in China: A view from outer space. *Journal of Urban*
773 *Economics*, *88*, 50–66. https://doi.org/10.1016/j.jue.2015.05.001
774 Emanuel, K. (2011). Global Warming Effects on U.S. Hurricane Damage. *Weather,*
775 *Climate, and Society*, *3*(4), 261–268.
776 https://doi.org/10.1175/WCAS-D-11-00007.1
777 Emanuel, K. A. (2013). Downscaling CMIP5 climate models shows increased tropical
778 cyclone activity over the 21st century. *Proceedings of the National Academy*
779 *of Sciences*, *110*(30), 12219–12224. https://doi.org/10.1073/pnas.1301293110
780 Geiger, T., Frieler, K., & Levermann, A. (2016). High-income does not protect
781 against hurricane losses. *Environmental Research Letters*, *11*(8), 084012.
782 https://doi.org/10.1088/1748-9326/11/8/084012
783 Geiger, T., Frieler, K., & Bresch, D. N. (2018). A global historical data set of tropical
784 cyclone exposure (TCE-DAT), 10. https://doi.org/10.5194/essd-10-185-2018
785 Holland, G. (2008). A Revised Hurricane Pressure–Wind Model. *Monthly Weather*
786 *Review*, *136*(9), 3432–3445. https://doi.org/10.1175/2008MWR2395.1
787 Howard, R. A., Matheson, J. E., & North, D. W. (1972). The Decision to Seed
788 Hurricanes: On the basis of present information, the probability of severe
789 damage is less if a hurricane is seeded. *Science*, *176*(4040), 1191–1202.
790 https://doi.org/10.1126/science.176.4040.1191
791 Iman, R. L., Johnson, M. E., & Watson Jr., C. C. (2005). Sensitivity Analysis for
792 Computer Model Projections of Hurricane Losses. *Risk Analysis*, *25*(5), 1277–
793 1297. https://doi.org/10.1111/j.1539-6924.2005.00673.x
794 Knapp, K. R., Kruk, M. C., Levinson, D. H., Diamond, H. J., & Neumann, C. J.
795 (2010). The International Best Track Archive for Climate Stewardship
796 (IBTrACS): Unifying Tropical Cyclone Data. *Bulletin of the American*
797 *Meteorological Society*, *91*(3), 363–376.
798 https://doi.org/10.1175/2009BAMS2755.1
799 Knapp, K. R., Diamond, H. J., Kossin, J. P., Kruk, M. C., & Schreck, C. J. (2018).
800 International best track archive for climate stewardship (IBTrACS) project,
801 version 4. *NOAA National Centers for Environmental Information*.

802 Knutson, T. R., McBride, J. L., Chan, J., Emanuel, K., Holland, G., Landsea, C., et al.
803 (2010). Tropical cyclones and climate change. *Nature Geoscience*, *3*(3), 157–
804 163. https://doi.org/10.1038/ngeo779
805 Lu, X., Yu, H., Ying, M., Zhao, B., Zhang, S., Lin, L., et al. (2021). Western North
806 Pacific Tropical Cyclone Database Created by the China Meteorological
807 Administration. *Advances in Atmospheric Sciences*, *38*(4), 690–699.
808 https://doi.org/10.1007/s00376-020-0211-7
809 Mendelsohn, R., Emanuel, K., Chonabayashi, S., & Bakkensen, L. (2012). The impact
810 of climate change on global tropical cyclone damage. *Nature Climate Change*,
811 *2*(3), 205–209. https://doi.org/10.1038/nclimate1357
812 Nordhaus, W. D. (2006). The economics of hurricanes in the United States. National
813 Bureau of Economic Research Cambridge, Mass., USA.
814 Nordhaus, W. D. (2010). The economics of hurricanes and implications of global
815 warming. *Climate Change Economics*, *01*(01), 1–20.
816 https://doi.org/10.1142/S2010007810000054
817 Pielke, R. A. (2007). Future economic damage from tropical cyclones: sensitivities to
818 societal and climate changes. *Philosophical Transactions of the Royal Society*
819 *A: Mathematical, Physical and Engineering Sciences*, *365*(1860), 2717–2729.
820 https://doi.org/10.1098/rsta.2007.2086
821 Sandel, B. (2015). Towards a taxonomy of spatial scale-dependence. *Ecography*,
822 *38*(4), 358–369. https://doi.org/10.1111/ecog.01034
823 Sealy, K. S., & Strobl, E. (2017). A hurricane loss risk assessment of coastal
824 properties in the caribbean: Evidence from the Bahamas. *Ocean & Coastal*
825 *Management*, *149*, 42–51. https://doi.org/10.1016/j.ocecoaman.2017.09.013
826 WMO (World Meteorological Organization). (2015). *Typhoon Committee operational*
827 *manual 2015*. Retrieved from
828 https://library.wmo.int/doc_num.php?explnum_id=7633
829 Sun, B., & Wang, H. (2015). Inter-decadal transition of the leading mode of
830 inter-annual variability of summer rainfall in East China and its associated
831 atmospheric water vapor transport. *Climate Dynamics*, *44*(9–10), 2703–2722.

https://doi.org/10.1007/s00382-014-2251-0

UNISDR (United Nations International Strategy for Disaster Reduction). (2015). *Global Assessment Report on Disaster Risk Reduction 2015: Making Development Sustainable: the Future of Disaster Risk Management* (Vol. 4). UN.

Walsh, K. J., McBride, J. L., Klotzbach, P. J., Balachandran, S., Camargo, S. J., Holland, G., et al. (2016). Tropical cyclones and climate change. *Wiley Interdisciplinary Reviews: Climate Change*, *7*(1), 65–89. https://doi.org/10.1002/wcc.371

Ward, P. J., Blauhut, V., Bloemendaal, N., Daniell, J. E., de Ruiter, M. C., Duncan, M. J., et al. (2020). Review article: Natural hazard risk assessments at the global scale. *Natural Hazards and Earth System Sciences*, *20*(4), 1069–1096. https://doi.org/10.5194/nhess-20-1069-2020

Wu, J., Gao, X., Giorgi, F., & Chen, D. (2017). Changes of effective temperature and cold/hot days in late decades over China based on a high resolution gridded observation dataset. *International Journal of Climatology*, *37*, 788–800. https://doi.org/10.1002/joc.5038

Wu, J., Li, N., & Shi, P. (2014). Benchmark wealth capital stock estimations across China's 344 prefectures: 1978 to 2012. *China Economic Review*, *31*, 288–302. https://doi.org/10.1016/j.chieco.2014.10.008

Wu, J., Li, Y., Li, N., & Shi, P. (2018). Development of an Asset Value Map for Disaster Risk Assessment in China by Spatial Disaggregation Using Ancillary Remote Sensing Data: Asset Value Map for Disaster Risk Assessment. *Risk Analysis*, *38*(1), 17–30. https://doi.org/10.1111/risa.12806

Wu, J., Han, G., Zhou, H., & Li, N. (2018). Economic development and declining vulnerability to climate-related disasters in China. *Environmental Research Letters*, *13*(3), 034013. https://doi.org/10.1088/1748-9326/aaabd7

Wu, J, He, X., Li, Y., Shi, P., Ye, T., & Li, N. (2019). How earthquake-induced direct economic losses change with earthquake magnitude, asset value, residential building structural type and physical environment: An elasticity perspective.

862 *Journal of Environmental Management*, *231*, 321–328.
863 https://doi.org/10.1016/j.jenvman.2018.10.050
864 Ye, M., Wu, J., Liu, W., He, X., & Wang, C. (2020). Dependence of tropical cyclone
865 damage on maximum wind speed and socioeconomic factors. *Environmental*
866 *Research Letters*, *15*(9), 094061. https://doi.org/10.1088/1748-9326/ab9be2